Heliyon 10 (2024) e24251

Contents lists available at ScienceDirect

Heliyon

journal homepage: www.cell.com/heliyon

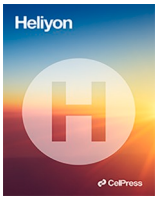

Research article

The impact of 180° return bend inclination on pressure drop characteristics and phase distribution during oil-water flow

Mushtaque Momin [a], Faisal Rahmani [a], Emad Makki [b], Mukesh Sharma [a,*], Jayant Giri [c], T. Sathish [d]

[a] Department of Mechanical Engineering, Birla Institute of Technology, Mesra, Ranchi, 835215, India
[b] Department of Mechanical Engineering, College of Engineering and Architecture, Umm Al-Qura University, Makkah 24382, Saudi Arabia
[c] Department of Mechanical Engineering, Yeshwantrao Chavan College of Engineering, Nagpur, India
[d] Saveetha School of Engineering, SIMATS, Chennai, 602105, Tamil Nadu, India

ARTICLE INFO

Keywords:
Liquid-liquid two-phase flow
Pressure drop
Superficial velocity
Gravitational effect
Phase distribution

ABSTRACT

The present work aims to capture the influence of the inclination of the return bend on flow patterns and pressure drop during oil-water flow. The experiments were carried out for different inclinations (0°, 15°, 30°, and 45°) of return bend for various superficial velocity combinations of oil (kerosene) and water ranging from 0.07 to 0.66 m/s. The experiments showed that pressure drop increases with the increase in inclination. However, the pressure drop at a fixed inclination (say 15°) decreases with the increase in the superficial velocity of the water. Distinct flow patterns observed in the return bend were droplet flow, film inversion, slug flow, plug flow and large slug flow. Droplet flow dominates at the lower range of kerosene (i.e., $U_{sk} = 0.07–0.2$ m/s) and higher range of water superficial velocity (i.e., $U_{sw} = 0.40–0.66$ m/s) at all the inclinations considered in this study. Additionally, comparisons between the experimental and numerical simulation results were made. The numerical solution utilized the Euler-Euler approach, considering the different phases as interpenetrating continua. The Volume of Fluid (VOF) model was used within this approach, monitoring the volume fraction of each phase over the domain while calculating one set of momentum equations for each phase. To capture the turbulent effects accurately, the k-ε turbulence model was incorporated. It happened to be found that the numerical findings showed remarkable agreement with the experimental data.

1. Introduction

In various industrial sectors such as petroleum, process, food, and chemical industries, the instances of two-phase oil-water (immiscible) flow through pipes and bends is an unavoidable phenomenon. U-bends are an essential component of the oil industry, as the flow through U-bends allows for the effective separation of water and oil [1]. The stratification that occurs when the mixed phase passes through the U-bend due to the difference in densities between the two phases could facilitate the extraction of water from the oil. Moreover, in a few oil production processes, emulsions (stable mixtures of oil and water) are formed. Where U-bends can be employed to break these emulsions by promoting coalescence, where water droplets combine into larger, separable volumes, aiding in the separation of oil and water [2]. U-bends are also used in pipeline integrity testing to evaluate the condition of pipelines

* Corresponding author.
E-mail addresses: eamakki@uqu.edu.sa (E. Makki), mukeshsharma@bitmesra.ac.in (M. Sharma).

https://doi.org/10.1016/j.heliyon.2024.e24251
Received 25 September 2023; Received in revised form 7 November 2023; Accepted 4 January 2024
Available online 8 January 2024

transporting oil and water. By examining the flow behaviour and conditions within a U-bend, operators can assess pipeline integrity and detect issues like blockages or erosion [3,4].

As a result, there has been a mounting curiosity among researchers to gain a comprehensive understanding of the liquid-liquid two-phase flow phenomena in these systems. However, prior studies on liquid-liquid flow through bends and pipes were inclined to concentrate mostly on horizontal straight tubes. A notable study by Arirachakaran et al. [5] revealed that an increase in oil viscosity leads to a decrease in the input water fraction required to invert the dispersion. Furthermore, it was observed that when the oil-water mixture in motion reached the inversion point, there was a significant and abrupt rise in pressure drop due to friction.

The significance of studying two-phase oil-water flow in pipes and bends stems from its pervasive presence across various industrial sectors. By gaining insights into the behaviour of this type of flow, industries can optimize their operations, improve efficiency, and ensure the smooth transportation of oil-water mixtures. Trallero et al. [6] and Zhang et al. [7] delved into the exploration of oil-water flow transition, which involves identifying two main classifications: segregated flow and dispersion flow. They employed a two-phase model specifically designed for light oil to predict this transition, effectively balancing gravitational forces with the turbulence occurring normally to the axial flow directions. A separate investigation by Al-Wahaibi et al. [8] focused on exploring the impact of viscosity, pipe diameter, and input velocities of both water and oil. They made a noteworthy discovery by utilizing an oil viscosity of 0.012 Pa-s. Specifically, they observed stratified flow in 19 mm and 25.4 mm diameter pipes transformed into bubbly and dual continuous flows at a specific oil velocity. However, when an oil viscosity of 0.0064 Pa-s was introduced in the 25.4 mm pipe, a significant observation was made that the transition to bubbly flow ceased, primarily due to the low Eotvos Number associated with the flow conditions. Furthermore, Poesio et al. [9] conducted a comprehensive study on the pressure drop variation in core annular flow, widely recognized as the most desirable flow pattern for transporting viscous oil. This pattern boasts several advantages, including a low power requirement by the pumps involved in the transportation process. Moreover, the CFD studies on the gas-liquid plug two-phase flow in a horizontal pipe were done using the standard k-ε turbulence model for a large diameter pipe having an internal diameter of 26 mm [10]. It was observed that the temporal variation of liquid hold-up in the plug flow is greatly influenced by the superficial gas velocity i.e., it fluctuates significantly with an increase in the superficial gas velocity. The formation of a small bubble in the gas phase causes significant fluctuation. The researchers proposed a model specifically tailored for accurate pressure drop calculations in a particular flow pattern, contributing valuable insights to the field. Similarly, Al-Wahaibi et al. [11] presented a model for calculating pressure drop in oil-water flow, specifically focusing on a separated model by fitting a Fanning friction factor.

Meanwhile, Hasan et al. [12] investigated the behaviour of flow patterns in vertical straight pipes, employing the drift-flux approach and primarily examining higher water fractions such as bubbly or pseudo-slug flow through experimental means. Their findings revealed that, apart from the terminal rise velocity of bubbles or droplets, the in-situ volume fraction influenced the lighter oil phase's drift velocity. Further analysis of flow pattern distribution in vertical straight tubes was conducted by Jana et al. [13] utilizing a conductivity probe technique and employing three different probe designs. The study indicated that at low flow rates of kerosene, a droplet flow pattern was observed within a continuous water phase. In contrast, the possibility of separated flow patterns, such as core annular flow, with a thin film of water near the wall, emerged at higher flow rates. In a study by Du et al. [14], the investigation focused on oil-water flow through a 20 mm diameter pipe. The researchers employed a mini-conductance probe and a VMEA sensor, proposing a time-frequency method to calculate and characterize the volume fraction and flow behaviour, respectively. Meanwhile, Xu et al. [15] conducted experimental research on pressure drop and phase inversion points in vertical pipes for upward and downward flow conditions. They specifically studied the flow transition behaviour from oil in water to water in oil. They discovered that the frictional pressure gradient reached its lowest value within the considered range at the phase inversion point. Furthermore, a numerical analysis has been done for a two-phase annular flow toward the onset of liquid film reversal in a vertical pipe. The phenomenon of film reversal in an annular flow in a vertical pipe was studied having a large diameter of 76.2 mm using the multi-fluid VOF method [16]. The standard k-ε turbulence model was also employed for capturing the turbulence effect with enhanced wall treatment. It was observed that there were irregular up-and-down liquid film flow waves near the pipe wall with a considerable amplitude when the superficial gas velocity drops. As a result, at a given superficial liquid velocity, there is an increase in the production of flooding waves with decreasing superficial gas velocities. This causes the liquid layer adhering to the pipe wall to thicken and become much more disturbed.

These studies contribute valuable insights into understanding vertical pipes' oil-water flow dynamics, including pressure drop calculations, flow pattern behaviour, volume fraction characterization, and phase inversion points. Despite the frequent occurrence of return bends in various process industries, relatively limited research has been conducted on the hydrodynamic behaviour of liquid-liquid flow, specifically in return bends. Most existing studies have predominantly focused on analyzing gas-liquid flow through bends, leaving a gap in understanding the specific characteristics of liquid-liquid flow in this type of pipe fitting. Ma et al. [17] conducted an experimental study employing the power spectral density technique to identify flow patterns in U-bends to address this gap. Meanwhile, López et al. [18], Wang et al. [19], and Yadav et al. [20] employed the photographic technique to identify flow patterns in various contexts. Additionally, Aliyu et al. [21] conducted an experiment on measurements of film thickness and investigated flow pattern transitions at different flow rates. Understanding the impact of U bends on pressure drop has also received attention in the literature. De Kerpel et al. [22] conducted a study measuring the effect of U bends on pressure drop for both downward and upward flow orientations. This research aimed to uncover the influence of U bends on the overall hydraulic performance of the system. These studies contribute to expanding the knowledge and understanding of liquid-liquid flow behaviour in return bends, including flow pattern identification, film thickness measurements, flow pattern transitions, and the effect of U bends on pressure drop. Further exploration of these phenomena is necessary to enhance the comprehension and optimization of liquid-liquid flow through return bends in process industries. On the contrary, minimal research has been conducted on the hydrodynamic behaviour of liquid-liquid flow passing through return bends in horizontal orientation. For instance, a study by Sharma et al. [23,24] investigated the flow transition of low and high viscous two-phase oil-water flow. The study examined two types of return bends: Rectangle bend and U

return bend. It also analyzed the variation in pressure drop caused by the bends. The results indicated that an increase in flow rate for low viscous oil led to an escalation in frictional pressure drop. Additionally, with its sharp change in the flow direction, the rectangular bend exhibited a higher pressure drop than the simple return bend in the case. The researchers also observed that the bend's geometry affects the downstream flow of all patterns. However, the change in flow direction did not impact the flow regime in the bend or its subsequent downstream. Furthermore, a CFD analysis was carried out by Das et al. [25] to examine the lubricating oil-water flow in U bend applying the k-ε turbulence model, specifically focusing on the core annular flow, which is highly desirable for oil transportation. The analysis revealed that the core annular flow exhibited a lower tendency for fouling in the up-flow configuration than in horizontal and downflow orientations.

Few recent studies on CFD analysis were also done by applying the k-ε turbulence model by Dutta et al. [26–28] on the turbulent flow separation and reattachment flow in pipe bends with different small curvature ratios and Reynolds number, turbulent vortex flow and turbulent flow field in a 90° pipe bend. They found that the flow separation takes place in the inner wall of these bends, and under various Reynolds numbers and curvature ratios, this separation zone goes up and down over time. Furthermore, CFD modelling was used for the study of pipe bend erosion for a two-phase liquid–solid slurry applying a standard k-ε model turbulence model [29]. The model has an internal diameter of 50 mm and a curvature ratio (2R/D) of 5.94 was studied. It was observed that Particle concentrations, flow velocities, and sizes have an impact on the erosion wear rate.

The preceding conversation suggests that researchers have consistently found the U return bend of great interest. Moreover, several research studies are available for oil-water flow through the return bends in a horizontal orientation. The information related to the inclined bend is essential as it may affect the flow pattern and pressure drop during oil-water flows. This information still needs to be made available. So, the current research aims to capture the effect of the inclination of the return bend on phase distribution and pressure drop characteristics during oil-water flows. Further, the experimental results were compared with the numerical model, which agrees with the experimental results.

2. Description of the experimental setup and procedure

The experimental setup, depicted in Fig. 1, comprises the necessary arrangements for experimenting effectively. The design includes a transparent acrylic U bend with an internal diameter of 0.008 m and a curvature ratio of ($2R/D = 7.5$), where R represents the radius of curvature (0.03 m). D represents the inner diameter of the test section, as illustrated in Fig. 1. In the experimental set-up, two horizontal pipes connected with the 180° return bend had a 1 m length of each tube. The test section is placed in the vertical plane and attached with a wooden board to provide the inclination mechanism for varying from −90° to +90°. The test fluids for the experiments were kerosene oil and water kept in two storage tanks **(14)** and **(16)** respectively shown in Fig. 1. These test fluids were pumped with the help of a centrifugal pump having a maximum discharge capacity of 4.16×10^{-4} m^3/s and a pressure head of 176.58 kPa in the test section. At the inlet of the test section, a special arrangement is made so that the test fluids can flow simultaneously in the test rig. In the test section, the fluids were pumped with the help of a submersible pump.

After coming out of the test rig, the mixture of these fluids was collected in a collection tank **(5)** where the kerosene oil and water separated due to density differences. As the density of water is higher than kerosene, it settled at the bottom of the tank, which was drained with the help of a drain valve **(8)** and collected into the water reservoir as shown in Fig. 1. The kerosene oil was drained with

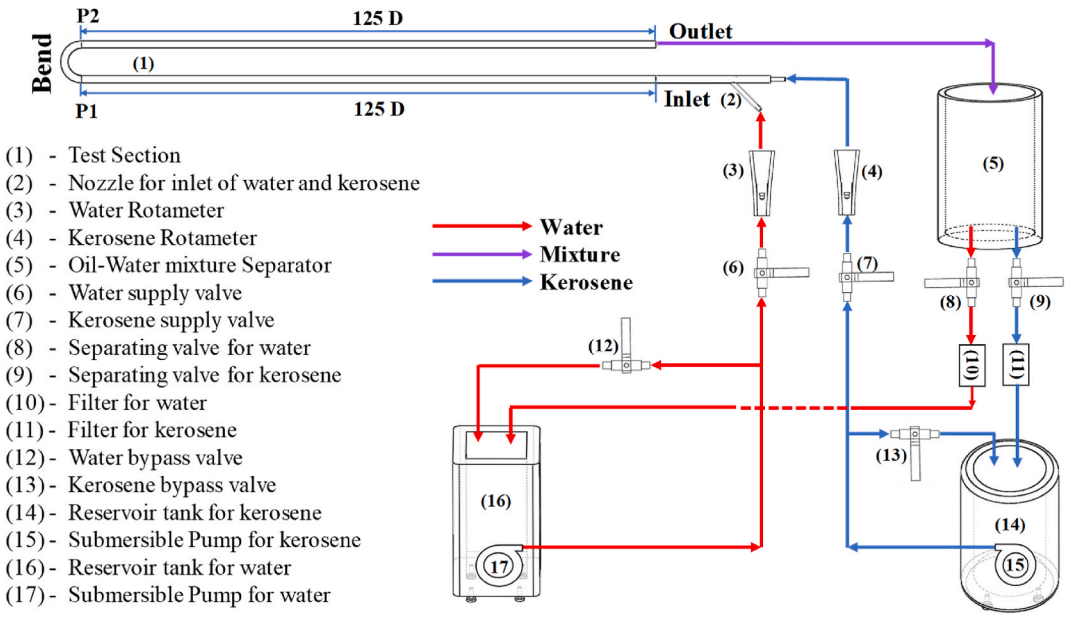

Fig. 1. U bend's schematic arrangement depicts the two-phase flow of kerosene oil and water.

the help of a drain valve **(9)** provided for kerosene oil and collected in the kerosene storage tank. Before collecting into the storage tanks or reservoirs, the kerosene oil and water were filtered **(10, 11)** to remove any dirt for better visual results. Kerosene and water used in this experiment have a density of 788 kg/m^3 and 960 kg/m^3, respectively, at atmospheric temperature and pressure. The viscosity of oil and water was 0.0012 Pa-s and 0.001 Pa-s, respectively. The interfacial surface tension between the kerosene oil and water was 0.022 N/m. The inflow of working fluids was controlled by two valves one was the main valve or supply valve **(6, 7)**, and another was the bypass valve **(12, 13)** which is connected to the respective storage tanks or reservoir **(14, 16)** and measured with the help of a rotameter **(3, 4),** as shown in Fig. 1. Both the rotameters were calibrated before experimenting. The measuring range of the rotameter is 0–3.33 $\times$ 10^{-5} m^3/s, with 3.33 $\times$ 10^{-6} m^3/s being the least count. The manufacturer supplied the measurement accuracy of the rotameter is $\pm$3 %, which was verified through calibration. The rotameter was calibrated with the help of a graduated cylinder and a stopwatch. The superficial velocities (U_s) of kerosene oil and water varied from 0.07 m/s to 0.66 m/s to observe various flow patterns due to changes in U_s keeping one phase constant.

The flow patterns were captured by varying the superficial velocities (U_s) of kerosene oil keeping water velocity constant ranging from (U_s 0.07 m/s to 0.66 m/s) with the help of a DSLR Canon EOS 5D MARK 3 high-speed camera with a maximum resolution of 5616 $\times$ 3744 pixels placed at a reasonable distance from the test section. An illumination source has been provided for better capturing.

The camera was installed on the tripod and the test section was brightened with the help of LED lights to capture the photographs and kept at a distance of 1.2 m for better visualization from the test section. The test section was configured at four different inclinations with the help of a special rotational mechanism provided on the wooden board, to analyze (0°, 15°, 30°, and 45°), as illustrated in Fig. 2. To analyze the influence of inclination on flow behaviour and pressure drop. A GEMS 3100 pressure transducer with an accuracy of $\pm$0.25 % was provided to determine the pressure drop across the bend.

3. Numerical methodology

3.1. Model development

The geometry of the model is shown in Fig. 3. It consists of a U-shaped tube with an internal diameter (D) of 0.008 m with a curvature ratio of 7.5. The two immiscible fluids, namely kerosene and water, are introduced into the tube coaxially, as shown in Fig. 4. The kerosene oil, characterized by a viscosity of 0.0012 Pa-s and a 788 kg/m^3 density, is injected at the central region. In contrast, water, with a viscosity of 0.001 Pa-s and a 960 kg/m^3 density, is introduced at the outer annular perimeter.

To simulate the transient flow of two fluids in a U-bend, the software Ansys Fluent 2023 R1 was used. The technique of finite volumes was used to discrete the governing mathematical equations. The modelling of multiphase flows in computational fluid dynamics (CFD) can be done using the Eulerian-Eulerian and Lagrangian-Eulerian approaches. The Lagrangian-Eulerian method considers the carrier fluid as a continuous form and solves the time-averaged Navier-Stokes equations. Meanwhile, the scattered phase is tracked by employing multiple particles. Alternatively, the Eulerian-Eulerian method mathematically handles the distinct phases by incorporating appropriate modifications for interphasic interactions.

For modelling the hydrodynamics of flow patterns in a U-bend, the volume of fluid (VOF) method available in Ansys Fluent is well-suited as the fluids are immiscible [10,16,25,30]. The VOF formulation assumes that multiple phases or fluids remain separate and do not mix. The volume fraction of each liquid is tracked within each computational cell across the entire domain. The sum of all phase's fractions equals one in each control volume. Each phase's physical properties and variables allocate its variables and physical properties. As long as the volume fraction of each phase is known for every control volume, the representation can be done using volume-averaged values.

The computational domain was messed with the help of the ANSYS 2023R Workbench, as seen in Fig. 4. There are 152,060 hexahedral elements. The two-phase pressure drop, as determined by the mesh independence test, does not appreciably alter, although the number of elements decreased from 296,854 to 152,060. Because of this, the final grid of 152,060 elements is accurate enough to be employed, which reduces processing time.

3.2. Grid Independence Test

Water and kerosene were the working substances for a grid independence study. The objective was to determine the optimal grid

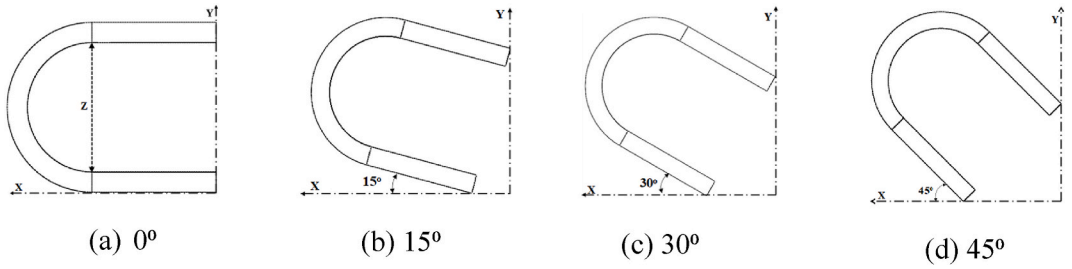

Fig. 2. Schematic representation of U-bend at different inclinations.

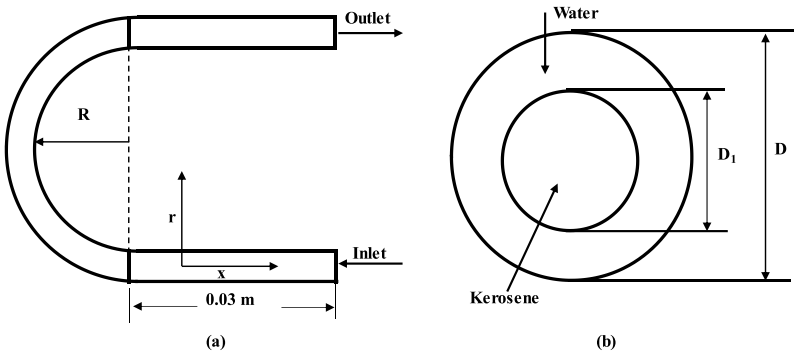

Fig. 3. Physical model of the test section (a) The front view. (b) The cross-sectional view.

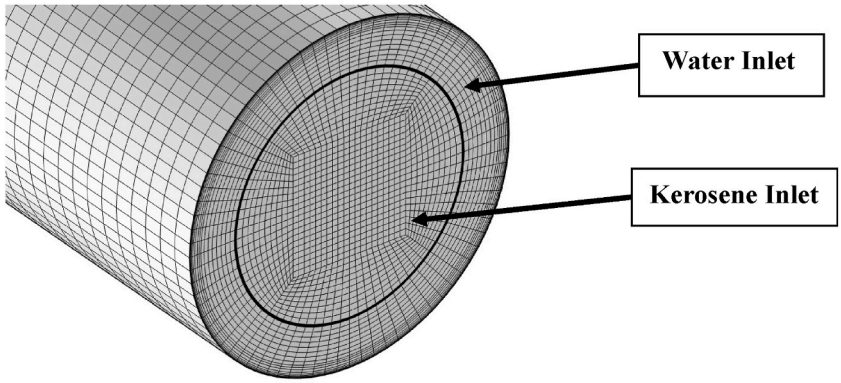

Fig. 4. Meshing of the inlet portion of U bend.

size for the present study. The effects of four different grid sizes, 56,224, 96,584, 152,060, and 296,854, were examined on the estimated total pressure drop across the U bend. The results showed that beyond a grid size of 152,060, there was no significant change in the pressure drop across the bend, as depicted in Fig. 5. Consequently, for the current study, a grid size of 152,060 was selected to

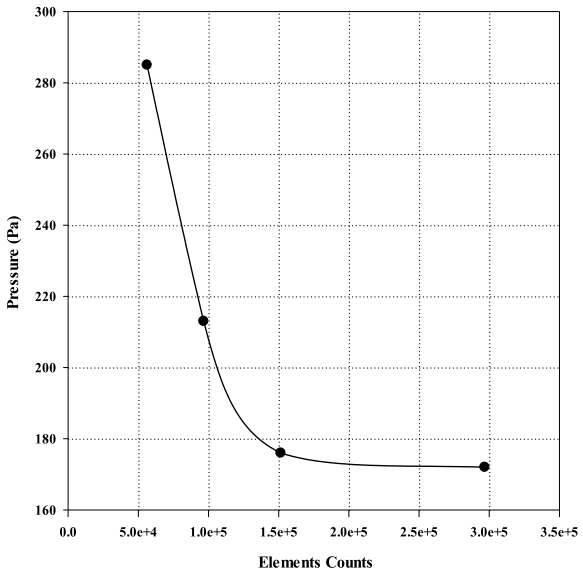

Fig. 5. Grid independence test.

perform all simulations, optimizing computational time. A reasonable grid resolution has been selected for the present simulation. Also, the difference in the pressure drop value at different grid counts was found to be less than 5 % which is an acceptable range [27].

3.3. Governing equations

The equation of continuity is expressed as follows:

$$\frac{\partial \rho}{\partial t} + \nabla.(\rho.U) = \sum_{q} S_q \tag{1}$$

Where ρ, U, t and S are density, velocity, time, and source term, respectively. In the current case, S is zero.

3.3.1. The momentum equation

By individually analyzing each phase and considering the interfacial forces between them, the equations governing the conservation of momentum in two-phase flow were derived. This equation expresses the volume-averaged velocities of each phase and incorporates the interfacial forces.

$$\frac{\partial(\rho U)}{\partial t} + \nabla.(\rho.U.U) = -\nabla P + \nabla.\ \left[\mu\left(\nabla U + \nabla U^{T}\right)\right] + (\rho g) + F \tag{2}$$

U is the velocity of the kerosene and water mixture, P is the flow field of pressure, g is the acceleration caused by gravity, F is the influence of body force experienced by the system and μ is flowing fluid viscosity.

Equations (1) and (2) can be utilized to estimate the density and viscosity of the fluid.

$$\rho = \sum_{1}^{N} \rho_q \alpha_q \tag{3}$$

$$\mu = \sum_{1}^{N} \alpha_q \mu_q \tag{4}$$

The phase fraction of the qth phase, denoted as α_q, is taken into account. A distinct equation of continuity for α_q is formulated as follows.

$$\frac{\partial \alpha_q}{\partial t} + \nabla.\left(\alpha_q u_q\right) = 0 \tag{5}$$

The given relationship holds true for each element.

$$\sum_{1}^{N} \alpha_q = 1 \tag{6}$$

The number of phases, denoted as N, allows for three potential conditions for α_q.

(1) $\alpha_q = 0$, The element does not include the qth fluid.
(2) $\alpha_q = 1$, the element is exclusively filled with the qth fluid along with one or more additional fluids.
(3) α_q ranges between 0 and 1 i.e., $0 < \alpha_q < 1$, means that the element exhibits an interface between the qth phase and other phases.

The Volume of Fluid (VOF) method employs a piecewise-linear approximation to determine the interface between fluids. This method assumes that the interface within each element has a linear slope. This method effectively calculates the fluid's advection across the faces of the elements by utilizing the linear shape. The initial step of interface reconstruction establishes the alignment of the linear interface concerning the centre of each partially filled element. This determination takes into account the volume fraction within the cell, as well as its derivatives. Subsequently, calculating fluid advection through every face involves utilizing the linear representation that was computed for the interface, which incorporates information about the distribution of normal and tangential velocities on the face. In the final step, the volume fraction within each cell is determined by reconciling the calculated fluxes from the previous step.

3.3.2. Turbulence model

The primary emphasis of this study is on the mean flow, despite the fact that the flow in the circular zone is turbulent. Therefore, the turbulence model was employed. The study utilizes the conventional k-ε model, which encompasses the two transport equations for viscous dissipation rate and turbulent kinetic energy as provided below.

$$\frac{\partial(\rho k)}{\partial t} + \nabla.(\rho \varepsilon u) = \nabla.\left(\left(\mu + \frac{\mu_t}{\sigma_s}\right)\nabla \varepsilon\right) + C_{1\varepsilon}\frac{\varepsilon}{k} 2\mu_t E_{ij} E_{ij} - C_{2\varepsilon}\rho\frac{\varepsilon^2}{k} \tag{7}$$

$$\frac{(\partial \rho k)}{\partial t} + \nabla.(\rho k u) = \nabla.\left(\left(\mu + \frac{\mu_t}{\sigma_k}\right)\nabla k\right) + 2\mu_t E_{ij} E_{ij} - \rho\varepsilon \tag{8}$$

In these equations, the variables k is turbulent kinetic energy, μ_t is eddy viscosity, and ε represents the dissipation rate. The values of k and ε are employed within the flow field to calculate the turbulent viscosity. Additionally, both k and ε are utilized in the momentum equation (2).

$$\mu_t = C_\mu \rho \frac{k^2}{\varepsilon} \tag{9}$$

E_{ij} used above is defined as

$$E_{ij} = \frac{1}{2}\left(\frac{\partial u_i}{\partial x_j} + \frac{\partial u_j}{\partial x_i}\right) \tag{10}$$

The constants are $C_\mu = 0.09$, $\sigma_k = 1.00$, $\sigma_\varepsilon = 1.30$, $C_{1\varepsilon} = 1.44$, and $C_{2\varepsilon} = 1.92$.

3.3.3. Surface Tension and wall adhesion

The Volume of fluid method incorporates the influence of interfacial surface tension between the phases. The interfacial surface tension method utilized in this study is derived from the continuum surface stress (CSS) method introduced by Lafaurie Bruno [31] within this model, the surface tension force is described by an equation that incorporates the unit tensor (I), the coefficient of surface tension (σ), and the tensor product ($\otimes$) of two vectors: the transformed normal and the original normal.

$$F_{css}.\left[\sigma\left(|\nabla.\alpha|I - \frac{\nabla\alpha \otimes \nabla\alpha}{|\nabla\alpha|}\right)\right] \tag{11}$$

The CSS method eliminates the need for explicit curvature calculations, making it particularly effective in under-resolved regions compared to other models. The current study focuses on the kerosene-water flow in a U-bend, which involves the presence of kerosene, water, and the surface of the pipe wall. The surface tension between kerosene and water is characterized using a coefficient of surface tension. Meanwhile, the contact angle is employed to characterize surface tension between the pipe wall and the fluid.

3.3.4. The fluid dynamic parameters

I. Equivalent Reynolds Number, Re_{eq}.

$$Re_{eq} = \frac{DU_{eq}\rho_{eq}}{\mu_{eq}} \tag{12}$$

$$U_{eq} = U_{sk} + U_{sw} \tag{13}$$

Where D is the inner diameter of U bend, U_{eq} is the equivalent velocity, and where U_{sk} and U_{sw} are the velocity of kerosene and water, respectively. ρ_{eq} is the equivalent density and can be calculated using the equation below:

$$\rho_{eq} = \frac{\rho_k U_{sk}}{U_{sk} + U_{sw}} + \frac{\rho_w U_{sw}(1.35U_{sk} + U_{sw}}{(U_{sk} + U_{sw})^2} \tag{14}$$

Whereas μ_{eq} is equivalent viscosity.

$$k_{tp} = \frac{2\Delta P_{hydro}}{\left(\rho_{eq} U_{eq}{}^2\right)} \tag{15}$$

II. The two-phase loss coefficient, k_{tp}

III. The average kerosene volume fraction, weighted by the respective areas, α_k

$$\alpha_k = \frac{1}{A}\sum_{i=1}^{n} \alpha_{ki} A_i \tag{16}$$

where A_i is the area occupied by the kerosene and A is the total cross-sectional area of the tube.

3.4. Boundary conditions

The axial and radial directions are denoted by the subscripts x and r, respectively. The kerosene phase and the water phase, respectively, are represented by the letters kerosene (k) and water (w), respectively, in Fig. 3.

3.4.1. Boundary circumstances at an inlet

The core area is where the kerosene velocity is represented, while the annular area shows the water velocity. The initial conditions are in the case of a velocity that has a uniform distribution.

At $x = 0.03$ m and $0 \leq r \leq 0.0056$ m, $U_r = 0$ and $U_x = U_{sk}$. (Fig. 3).

At $x = 0.03$ m and 0.0056 m $\leq r \leq 0.008$ m, $U_r = 0$ and $U_x = U_{sw}$. (Fig. 3).

3.4.2. Wall boundary conditions

A fixed, non-slipping ($U_x = 0$), and non-penetrating ($U_r = 0$) boundary is established on the pipe wall. Additionally, the acrylic resin used to make the pipe walls has a contact angle (27°) with the water at the wall.

3.4.3. Boundary circumstances at an outlet

The pipe has a backflow turbulence intensity of 5 % and a backflow hydraulic diameter of 0.008 m. Furthermore, a pressure outlet boundary has been defined for the pipe.

3.5. Methods of discretization and the convergence condition

A transient simulation is carried out with a time step of 0.001s in order to take the unpredictable nature of the two-phase flow into account. Various discretization methods are employed for the governing equations. The continuity equation utilizes the PRESTO scheme [32] while a second-order upwind scheme is employed for momentum. For turbulent kinetic energy and dissipation rate, a first-order upwind method is utilized. The SIMPLE (Semi-Implicit Method for Pressure Linked Equation) algorithm is used to carry out pressure-velocity coupling [33] The residual values of important variables, such as mass, velocity components, and volume percentage, are used to establish convergence criteria. The convergence criteria in this study are set at 10^{-4} for all variables.

4. Result and discussions

An experimental and numerical study has been done on U bend in four different inclinations, i.e., 0°, 15°, 30°, and 45°. In this study, the effect of the superficial velocity of the fluids on the phase distribution has been studied. The impact of inclinations on the phase distribution and pressure drop variation across the bend was studied.

4.1. Effect of inclination and superficial velocity on phase distribution

A comprehensive experimental study of flow patterns for two immiscible liquids (oil-water) was performed in U bend at different inclinations. Figs. 6–9 shows the flow regime developed for different inclinations of U bend, i.e., at 0°, 15°, 30°, and 45°°. It can be noted that the flow patterns were strongly affected by the superficial velocities of fluids and inclination as well. In the case of 0° orientation, the change in the superficial velocity of kerosene oil and water mostly results in film inversion, droplet flow and slug flow. The film inversion was noticed for kerosene oil-water velocity range $U_{sk} = 0.33$–0.66 m/s and $U_{sw} = 0.07$–0.66 m/s as the high flow rates and velocities of kerosene-oil and water results in turbulent conditions within the U-bend, leading to disturbances in the liquid film.

These disturbances can cause the film to break and invert. The slug flow characterized by the regular appearance of a bullet-shaped liquid phase, followed by a second liquid known as dispersed phase having clear distinct interfaces between the two phases. It was observed at $U_{sk} < 0.33$ m/s and $U_{sw} \leq 0.46$ m/s as low flow rate of kerosene-oil and high flow rate of water where kerosene slug was

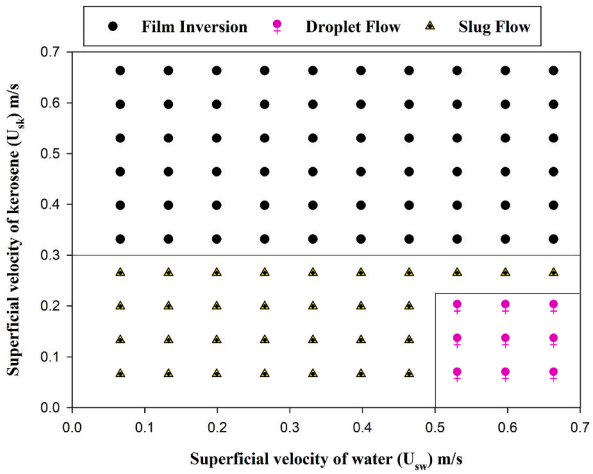

Fig. 6. Flow regime map of U bends with the superficial velocity at 0° inclination.

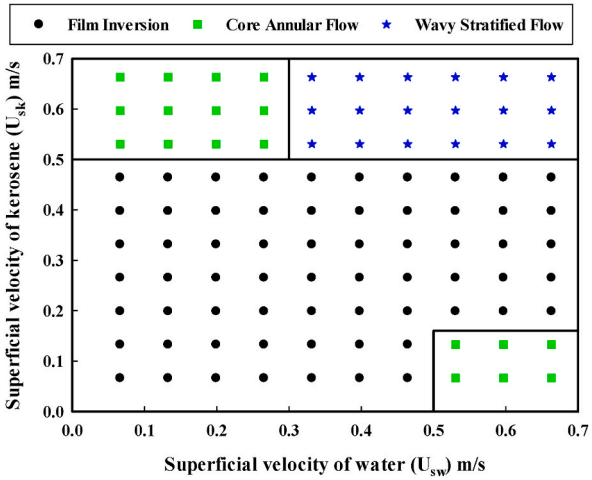

Fig. 7. Flow regime map of U bends with the superficial velocity at 15° inclination.

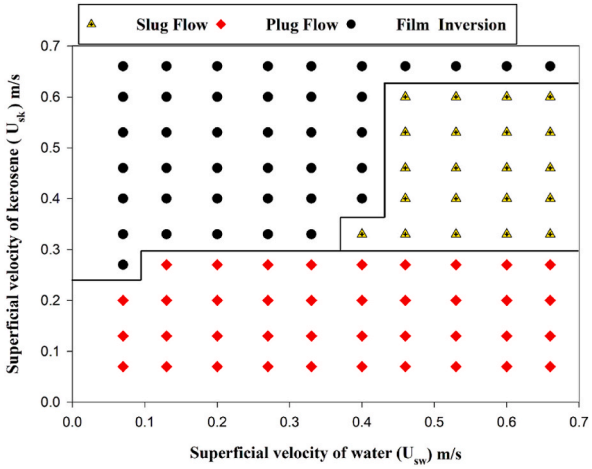

Fig. 8. Flow regime map of U bend with the superficial velocity at 30° inclination.

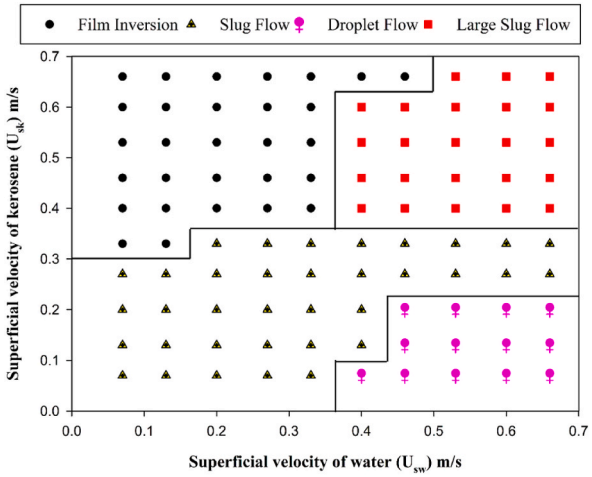

Fig. 9. Flow regime map of U bend with the superficial velocity at 45° inclination.

propelled forward by the momentum of the flow as shown in Fig. 11. A similar observation was also mentioned by Verma et al. [34] for low velocity ranges having the same density ratio of the working fluid (i.e., kerosene and water). The slug flow has a pulsating periodic nature, as it moves downstream can create pressure waves results sudden change in pressure drop can damage the engineering equipment.

The droplet flow is identified as dispersed liquid droplets in a continuous liquid phase as a result of differences in density and surface tension. It was observed at a low superficial velocity of kerosene $U_{sk} \leq 0.2$ m/s and high $U_{sw} \geq 0.46$ m/s, which can be seen in Figs. 6 and 11. Moreover, this can also be attributed to the high velocity of water and low velocity of kerosene oil, which induces the shear forces that cause the liquid interface to break, resulting in the formation of droplets. The study of droplet flow is very crucial in Liquid- Liquid Extraction or solvent extraction process to taking a specific material out of one liquid phase and putting it in another. Therefore, effective separation and mass transfer depend on the control of droplet size and dispersion.

Whereas at 15° inclination, the flow patterns observed were film inversion, wavy stratified and core annular flow. For $U_{sk} \geq 0.46$ m/s and $U_{sw} \geq 0.27$ m/s the core annular flow, described as the flow of two immiscible liquids via a conduit, with the usual arrangement of one liquid forming a core and the second liquid creating an annular layer around was observed. it was also observed in high velocity range of water and low velocity of kerosene i.e., $U_{sk} \leq 0.13$ m/s and $U_{sw} \geq 0.46$ m/s.

This can be attributed to the combined effect of the high difference between relative velocity of kerosene and water velocity, the interfacial tension between the phases and increase in the gravity force due to inclination of the bend. In operations involving the separation and mixing of two-phase flows in U-bends, the flow pattern is essential. As it also helps in the transportation of two-phase mixture. Therefore, accurate prediction is important for the equipment safety as well as for flow stability.

In the high range velocity of kerosene and water i.e., $U_{sk} \geq 0.33$ m/s and $U_{sw} \geq 0.46$ m/s wavy stratified flow was observed as the centrifugal force and gravity force balance each other resulted in the formation of the flow. The dominant flow pattern was film inversion, which can be seen in Fig. 7.

For 30° inclination, the flow patterns observed were slug flow, plug flow and film inversion. For $U_{sk} \leq 0.27$ m/s and $0.07 \text{ m/s} \leq U_{sw} \leq 0.66$ m/s plug flow pattern was observed. The low flow rate and velocity of the kerosene-water mixture play a significant role in the formation of plug flow. Also, the high interfacial tension promotes the separation of two phases and helps in maintaining the integrity of the kerosene plug.

With further increase in $U_{sk} \geq 0.33$ m/s and $U_{sw} \geq 0.46$ m/s, the transition of plug flow to slug flow takes place. At $U_{sk} \geq 0.33$ m/s and $U_{sw} \leq 0.40$ m/s due to the increase in the volume fraction of the kerosene, the slug merges and leads to the formation of film inversion, a unique flow pattern only observed in return bends or in curved conduits, described as the liquid passes through the U-bend, the liquid phase that was initially on the pipe's upper wall transforms into the lower film, and the liquid on the lower wall transforms into the upper film. In operations involving the separation and mixing of two-phase flows in U-bends, the flow pattern is essential such as chemical processing and petrochemical industries which can be seen in Fig. 8.

In addition to that, at 45° inclination the slug flow, film inversion, large slug and droplet flow patterns were observed. The film inversion flow pattern was observed in the range of $0.66 \geq U_{sk} \geq 0.4$ m/s and $0.07 \leq U_{sw} \leq 0.4$ m/s. This can be attributed to the momentum of the kerosene phase being higher as compared to water which leads the kerosene oil flow through outer wall of the bend and the water phase flows through the inner wall of the bend. Although the kerosene oil detached earlier from the upper wall of the tube due to gravity effect caused due to inclination of the tube as shown in Fig. 17. At $U_{sw} \geq 0.4$ m/s and $U_{sk} \leq 0.2$ m/s, droplet flow was observed. And at high velocity of kerosene oil and water, i.e., U_{sk} and $U_{sw} \geq 0.40$ m/s, respectively, a large slug flow pattern was observed.

The effect on flow patterns due to inclination of U bend can be observed as shown Fig. 10**.** The change in flow patterns were shown for constant rate of superficial velocities of kerosene oil and water. It clearly shows that as the inclination of U bend increases the flow patterns changes. At 0° the flow pattern observed is slug flow, but as the inclination increased the length of slug decreases.

Despite having the same flow pattern (slug flow) at 0° and 45° at constant velocities, the slug length and shape are not similar, indicating the effect of inclination on slug length.

The superficial velocity of kerosene oil and water also affects the flow patterns. Fig. 11 clearly indicates that, as the superficial velocity of kerosene changes 0.07 m/s to 0.53 m/s keeping the water velocity constant at 0.66 m/s the transition of droplet flow to film inversion happens at 0° inclination. Similarly, the transition of flow patterns happens due to change in superficial velocity for different

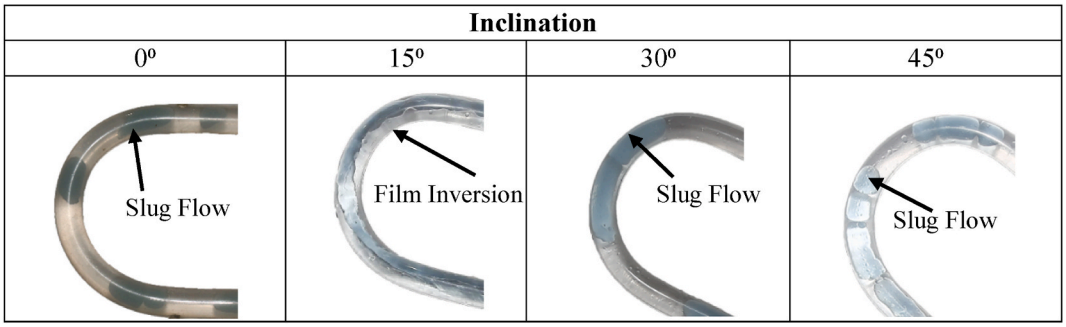

Fig. 10. Effect of inclination on flow patterns at constant superficial velocities $U_{sk} = 0.33$ m/s and $U_{sw} = 0.33$ m/s.

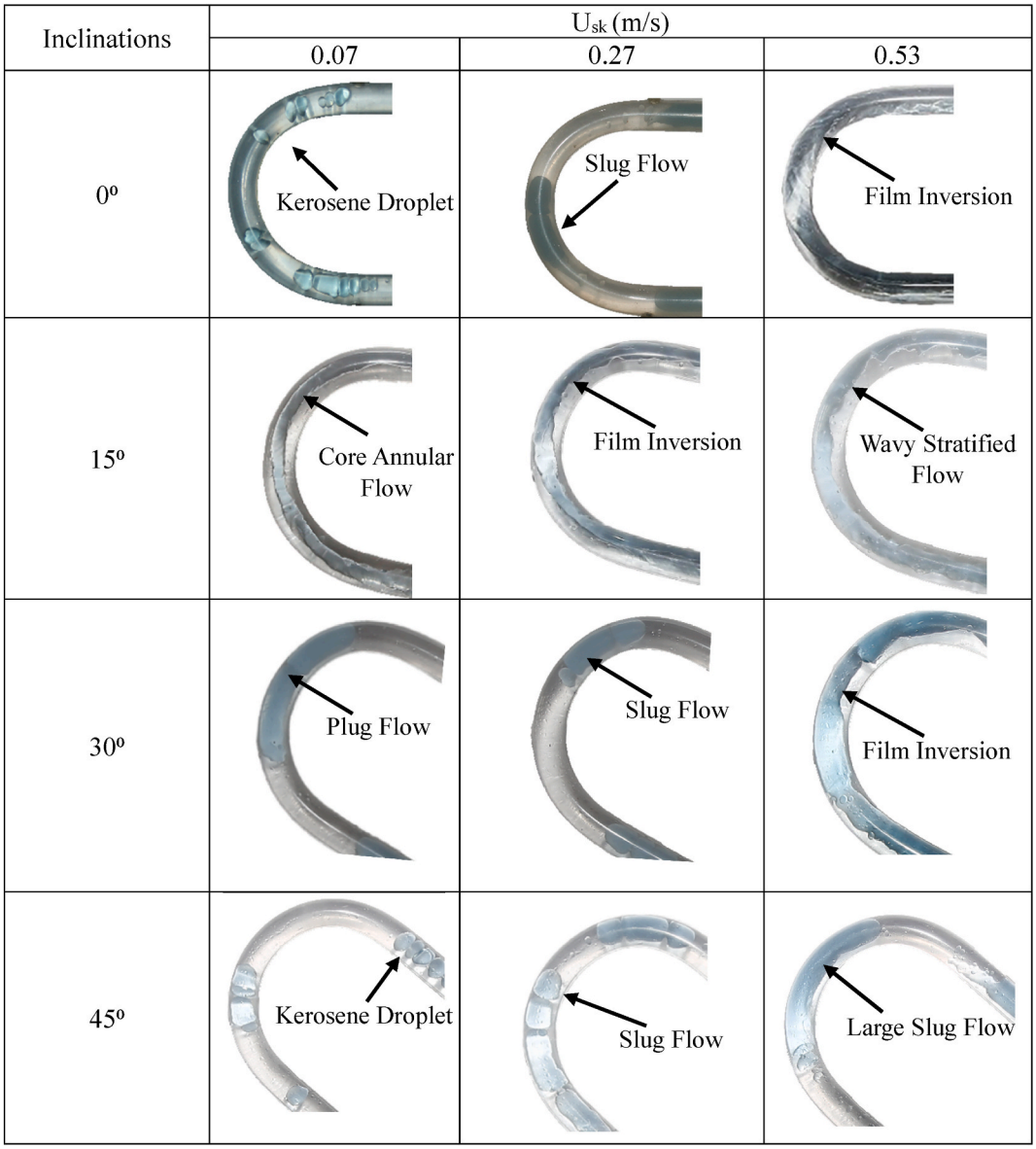

Fig. 11. Effect of superficial velocities on flow pattern at different inclinations at constant U_{sw} = 0.66 m/s.

inclinations i.e., 15°, 30° and 45°.

4.2. *Effect of inclination on pressure drop*

An attempt has been made to understand the distinctive characteristics of pressure drop across the U bend horizontally as well as the increase of inclination of the U bend in a clockwise direction, as shown in Fig. 2. The total pressure drop across the U bend is the amalgamated impact of wall friction of the bend (ΔP_f), gravity (ΔP_g) or static head and the change in momentum caused by the direction shift. i.e., bend loss (ΔP_{bend}). Thus mathematically,

$$\Delta \boldsymbol{P}_t = \Delta \boldsymbol{P}_f + \Delta \boldsymbol{P}_{\mathbf{g}} + \Delta \boldsymbol{P}_{bend} \tag{17}$$

By measuring the differential pressure drop over the bend, one may determine the total pressure drop ΔP_t, provided the static head or (ΔP_g) is obtained by.

$$\Delta P_g = +\rho_m g z \tag{18}$$

Where ρ_m is the mixture density, g is the acceleration due to gravity, z is the vertical distance between the pressure taps across the bend,

and the + sign indicates the up-flow direction of flow. It is difficult to calculate the pressure drop due to bend (ΔP_{bend}) and friction pressure drop (ΔP_f) separately. Therefore, to avoid the complexity, both the pressure loss is combined into a single pressure drop defined for the present case as hydrodynamic pressure drop (ΔP_{hydro}). Furthermore, (ΔP_{hydro}) can be calculated by subtracting the pressure drop due to the gravitational component from the total measured pressure drop across the bend. Therefore, it can be written as:

$$\Delta P_{hydro} = \Delta P_t - \alpha_k \, (\rho_w - \rho_k) g z \cos\theta \tag{19}$$

Where in-situ volume fraction and the liquid density are denoted by α and ρ, respectively, with the subscripts k and w denoting the water and kerosene phases. θ represents the angle between the reference line and the U bend, as shown in Fig. 2. As there are different methods and correlations available to calculate in-situ volume fraction. But most of the correlations were developed for straight tubes. For the slip-free model, which usually represents the homogeneous model. This model is generally applied to scattered two-phase systems. Such systems have flow patterns such as slug flow, bubbly flow or droplet flow considered continuous phase velocity. Based on this method, Pietrzak [35] proposed a correlation for U-bend to calculate the in-situ volume fraction for the horizontal tube. Therefore, to calculate α_k, which is the in-situ volume fraction of kerosene. The correlation is given as

$$\alpha_k = (\beta_k)^{0.6} \quad \alpha_w = 1 - \alpha_k \tag{20}$$

Where α_w represents the in-situ volume fraction of water, β_k represents the input volume fraction of kerosene. The input volume fraction of kerosene and water can be expressed with the help of the volume flow rate of Q_k and Q_w respectively.

$$\beta_k = \frac{Q_k}{Q_k + Q_w} \quad \beta_w = 1 - \beta_k \tag{21}$$

The function of Q_w/Q_k with U_{sk} as a parameter is used to illustrate the hydrodynamic pressure gradient $(\nabla P_h/L_b)_{bend}$ across the bend, where L_b is the bend length and the distance between the pressure taps across the bend.

Figs. 12–15 shows the hydrodynamic pressure drop $(\nabla P_h/L_b)_{bend}$ with respect to function Q_w/Q_k at different inclinations i.e., 0°, 15°, 30°, and 45°. It can be inferred from Figs. 12–15 that the pressure drop increases with the increase in the superficial velocity of water (U_{sw}) for a constant superficial velocity of kerosene (U_{sk}). Also, Figure show that the slope of pressure drop becomes steeper with the increase in U_{sk}. This trend is similar for all the inclinations.

From Fig. 12, it can be noted that the maximum pressure drop obtained at lower $U_{sk} = 0.07$ m/s is 2021 Pa/m at $Q_w/Q_k = 10$ while the maximum pressure drop at higher $U_{sk} = 0.66$ m/s is 3776 Pa/m at $Q_w/Q_k = 1$ for 0° inclination. Further, with the increase in the inclinations of the U- Bend, i.e., 15°, 30°, 45° (Figs. 13–15), an increase in the maximum pressure drop was observed for similar sets of U_{sk} and Q_w/Q_k. At 45° inclination (Fig. 15), the maximum pressure drop obtained for higher $U_{sk} = 0.66$ m/s at $Q_w/Q_k = 1$ is 4043 Pa/m. The increase in the maximum pressure drop from 0° to 45° is 267 Pa/m. This confirms that the inclination strongly affects the pressure drop across the bend. The increase in the pressure drop across the bend at different inclinations with respect to 0° for different sets of U_{sk} is depicted in Fig. 16.

Tables 1–4 shows the change in the percentage of pressure drop of U bend at different inclinations, i.e., 15°, 30°, and 45°, with respect to the 0° inclination for constant U_{sk}. It can be inferred from Table 1 that as the inclination angle of U bend increases the change in percentage of pressure drop increases.

5. Comparison of numerical model with experimental results

To validate the numerical model, Computational fluid dynamics simulations are performed for various combinations of operating

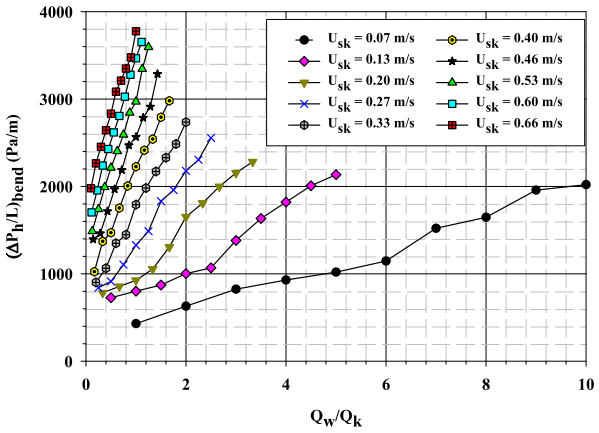

Fig. 12. Hydrodynamic Pressure drop variation of bend section with discharge ratio at 0° inclination.

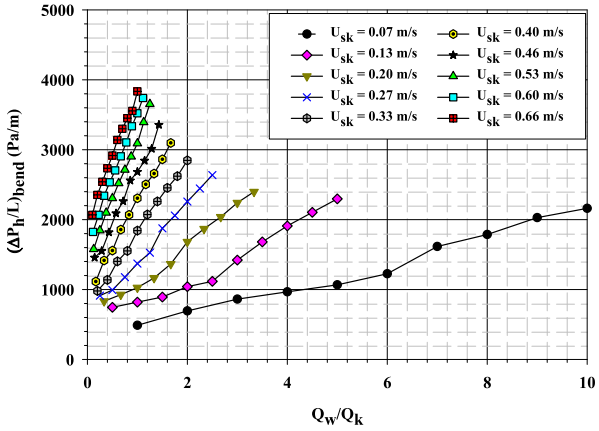

Fig. 13. Hydrodynamic Pressure drop variation of bend section with discharge ratio at 15° inclination.

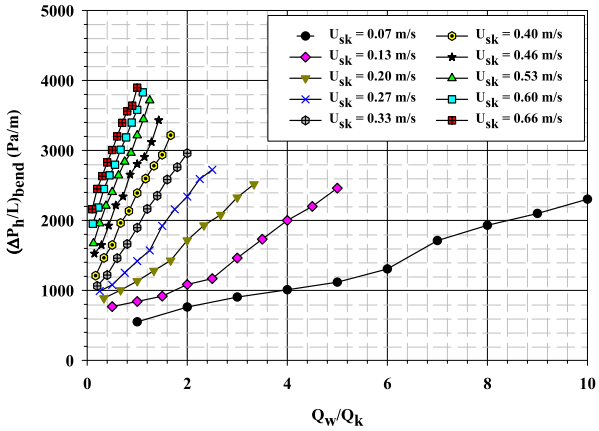

Fig. 14. Hydrodynamic Pressure drop variation of bend section with discharge ratio at 30° inclination.

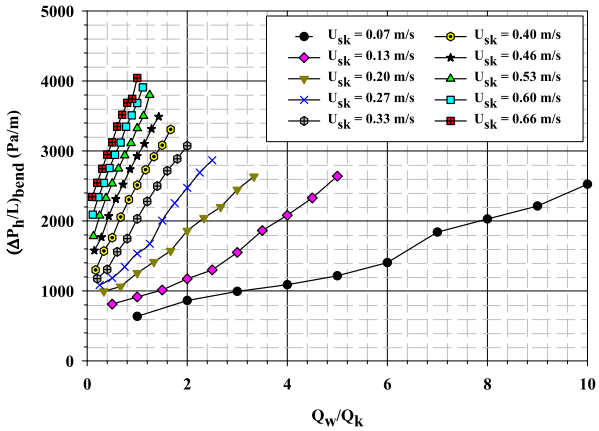

Fig. 15. Hydrodynamic pressure drop at bend section with discharge ratio at 45° inclination.

conditions. The flow pattern obtained from the numerical results are compared with the experimental observation, this process enables the assessment of the accuracy and reliability of the numerical model. The various flow patterns observed are shown in Figs. 17 and 18 for different combinations of superficial velocities of kerosene and water. To avoid repetition, two combinations of the superficial velocities of kerosene and water are shown.

The droplet flow at 0° inclination is in good agreement with the experimental results as the size of the kerosene droplets is

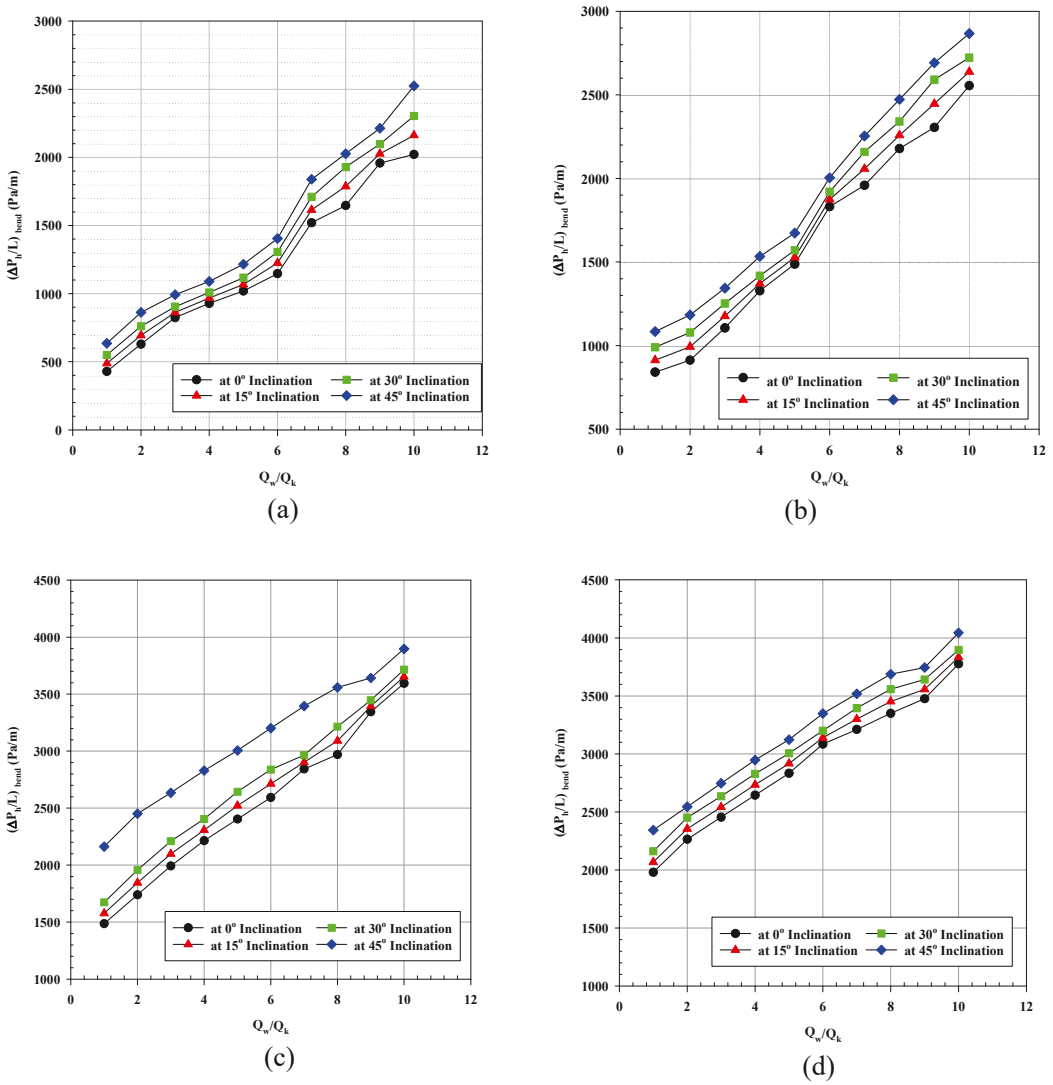

Fig. 16. Comparison of Hydrodynamic Pressure drop at different inclinations (a) at constant U_{sk} = 0.07 m/s (b) at constant U_{sk} = 0.27 m/s (c) at constant U_{sk} = 0.53 m/s (d) at constant U_{sk} = 0.66 m/s.

comparable to experimental results for the considered superficial velocity of kerosene oil and water, as shown in Fig. 17. Similarly, the film inversion was obtained at 15° inclination for both experimental and numerical study. This demonstrates that the numerical model and the experimental results are in good agreement.

The experimental and numerical pressure drop values at U_{sk} = 0.07 m/s & U_{sw} = 0.66 m/s, and U_{sk} = 0.66 m/s & U_{sw} = 0.66 m/s are tabulated in Table 5. A maximum of 4 % deviation in pressure drop was observed at U_{sk} = 0.07 m/s & U_{sw} = 0.66 m/s and 4.71 % at U_{sk} = 0.66 m/s & U_{sw} = 0.66 m/s, which is in the acceptable limit. So, it can be said that the numerical model is validated with experimental results.

Although the results obtained from the experimental study could have been generalized. If an ultra high-speed phantom TE2010 camera would have been used to capture every minor detail of flow patterns. However, the flow patterns that were captured are also good as the experiments were performed for many repetitions. Also, in the experimental setup up rotameter has been used to measure the volume flow rate although it is possible to have a human error while controlling the flow rate. Instead of the rotameter a Coriolis Flow Meter could have been used for very high accuracy. On the other hand, the numerical simulation of the present study has been done in a smaller dimension compared to the experimental model. The results may have considered the effects of the upstream and downstream length as the actual dimensions of the bend have been used in the experiment. However, the chances are very low as the study was only focused on the bend section, not on the entire domain and the experimental results showed good agreement with the numerical model. Sometimes it was observed that using different hardware and software resources may produce some error in terms of change in pressure data value or flow pattern behaviour.

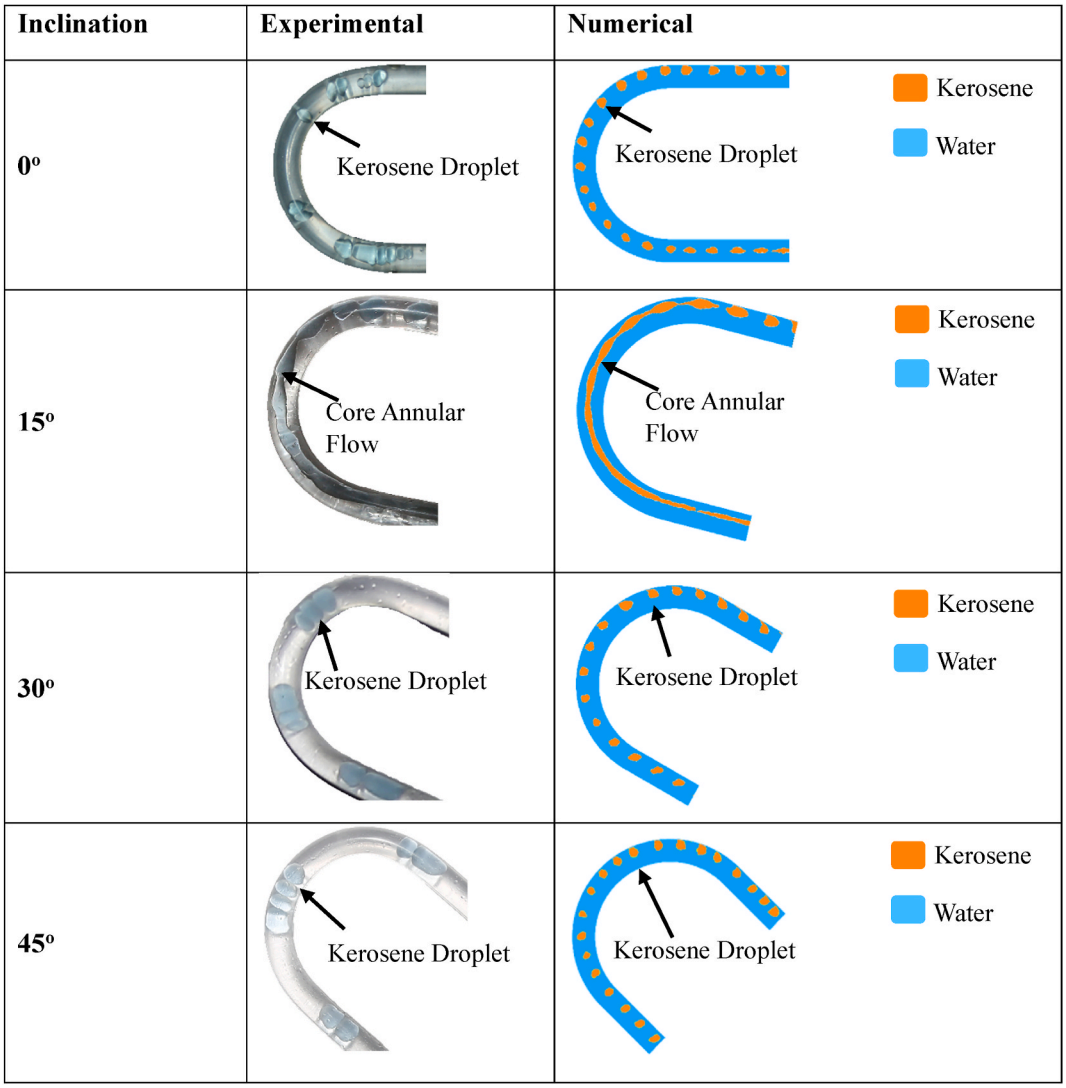

Fig. 17. Experimental and numerical flow patterns at different inclinations at $U_{sk} = 0.07$ m/s and $U_{sw} = 0.66$ m/s.

Table 1
Percentage increase in the pressure drop w.r.to 0° inclination for a $U_{sk} = 0.07$ m/s.

Superficial velocity (m/s)	% Change in Pressure Drop (w.r.to 0°)		
U_{sw}	at 15° inclination	at 30° inclination	at 45° inclination
0.07	13.64	28.22	47.97
0.13	10.19	20.88	36.93
0.20	4.73	9.79	20.40
0.27	4.17	8.60	17.25
0.33	4.70	9.60	19.25
0.40	6.87	13.91	22.44
0.46	6.19	12.50	20.95
0.53	8.54	17.17	23.07
0.60	3.53	7.15	13.05
0.66	6.95	13.97	24.88

Table 2
Percentage increase in the pressure drop w.r.to 0° inclination for a $U_{sk} = 0.27$ m/s. As shown in Table 1, For lower superficial velocity of kerosene ($U_{sk} = 0.07$ m/s) and water ($U_{sw} = 0.07$ Pa/m) percentage increase in the pressure drop, increases from 13.64 to 47.97 with the increase in inclination from 15° to 45° with respect to 0° inclination. This trend can be seen at sets of superficial velocities (Tables 2–4). This confirms that increase in inclination strongly affects the pressure drop across the bend section.

Superficial velocity (m/s)	% Change in Pressure Drop (w.r.to 0°)		
U_{sw}	at 15° inclination	at 30° inclination	at 45° inclination
0.07	8.53	17.70	28.91
0.13	8.85	18.22	29.75
0.20	6.43	13.26	21.56
0.27	3.24	6.78	15.49
0.33	2.67	5.59	12.49
0.40	2.33	4.85	9.40
0.46	5.02	10.21	15.07
0.53	3.65	7.45	13.51
0.60	6.14	12.40	16.77
0.66	3.23	6.57	12.19

Table 3
Percentage increase in the pressure drop w.r.to 0° inclination for $U_{sk} = 0.53$ m/s.

Superficial velocity (m/s)	% Change in Pressure Drop (w.r.to 0°)		
U_{sw}	at 15°° inclination	at 30° inclination	at 45° inclination
0.07	6.10	12.58	19.81
0.13	6.08	12.48	19.32
0.20	5.30	10.86	16.79
0.27	4.20	8.63	14.50
0.33	4.90	9.99	14.34
0.40	4.65	9.48	13.26
0.46	2.06	4.27	9.44
0.53	4.06	8.25	11.93
0.60	1.47	3.05	4.64
0.66	1.62	3.35	5.68

Table 4
Percentage increase in the pressure drop w.r.to 0° inclination for $U_{sk} = 0.66$ m/s.

Superficial velocity (m/s)	% Change in Pressure Drop (w.r.to 0°)		
U_{sw}	at 15° inclination	at 30° inclination	at 45° inclination
0.07	4.42	9.13	18.32
0.13	3.99	8.23	12.41
0.20	3.55	7.31	11.90
0.27	3.41	7.00	11.47
0.33	2.96	6.08	10.23
0.40	1.81	3.76	8.57
0.46	2.79	5.73	9.56
0.53	3.05	6.22	10.06
0.60	2.31	4.74	7.72
0.66	1.55	3.20	7.09

6. Conclusion

The experimental and numerical investigation was done on oil-water flow through return bends at four distinct inclinations, i.e., 0°, 15°, 30°, and 45°. The pressure drop characteristics and the flow regime has been studied. The following conclusion from the study can be drawn.

- The hydrodynamics as well as the pressure drop of the oil-water flow was greatly affected by the individual superficial velocity of the test fluids and the inclination of the bend. As the flow patterns changes and pressure drop increases with the increase of superficial velocity and inclination angle of U bend.
- Distinct flow patterns were observed in the study like film inversion, slug flow, plug flow, wavy stratified flow, and droplet flow. Interestingly, core annular flow was observed at 15° inclination only.
- It can be inferred from the flow regime graphs i.e., from Figs. 6, Figure 7, Figs. 8 and 9 that at 15° inclination, for velocity range of ($0.53 \leq U_{sk} \leq 0.66$ m/s & $0.07 \leq U_{sw} \leq 0.27$ m/s and ($0.07 \leq U_{sk} \geq 0.13$ & $0.53 \leq U_{sw} \leq 0.66$ m/s) is favourable for oil

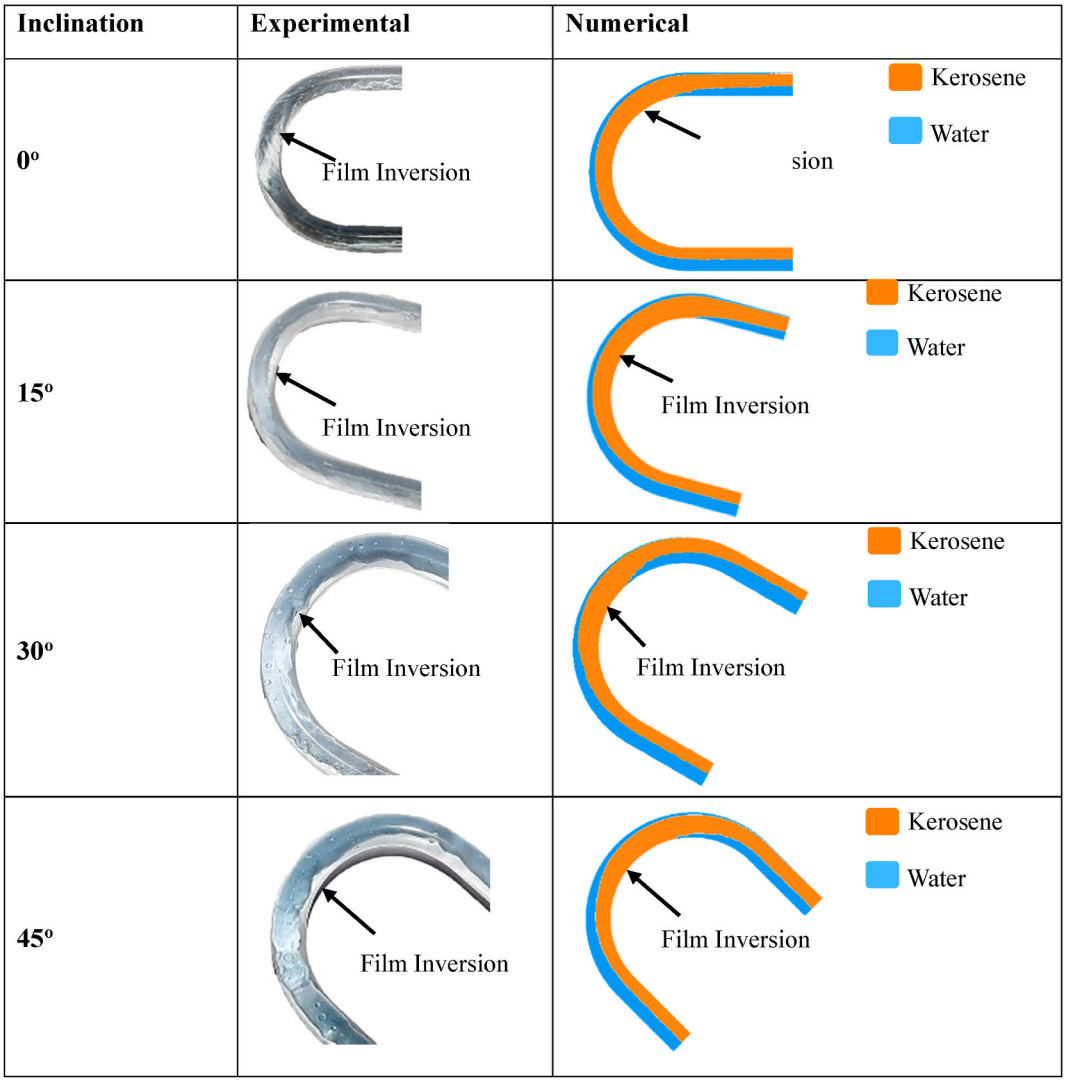

Fig. 18. Experimental and numerical flow patterns at different inclinations at U_{sk} = 0.66 m/s and U_{sw} = 0.66 m/s.

Table 5
Comparison of pressure drop obtained from experiment and numerical simulations at different inclinations.

Superficial velocity (m/s)		Inclinations	Pressure Drop (Pascals) (∇P)		Percentage Difference
U_{sk}	U_{sw}		Experimental	Numerical	
0.07	0.66	0°	192	200	4.00
		15°	205	212	3.30
		30°	218	226	3.54
		45°	239	242	1.24
0.66	0.66	0°	361	372	2.96
		15°	366	379	3.43
		30°	371	385	3.64
		45°	384	403	4.71

transportation as it provides core annular flow which is the most desirable flow pattern for two phase liquid-liquid flow. Although more experimental and numerical study needs to be explored for different bend inclinations and bend diameter to reach a generalized conclusion.

- The increase in the inclination of the U bend resulted in the increase in pressure drop across the U bend section. On increasing the angle 0° to 15°, the maximum increase in pressure drop was 13.64 % at $U_{sk} = 0.07$ m/s and $U_{sw} = 0.07$ m/s, while at 45° the increase in pressure drop was 47.97 %. This confirms that the increase in inclination strongly affects the pressure drop across the bend section.
- The increase in pressure drop reduces with the increase in U_{sk}. At $U_{sk} = 0.27$ m/s and $U_{sw} = 0.07$ m/s, the percentage increase in pressure drop was 8.53 % at 0°, 17.70 % at 30° and 28.91 % at 45°. Similarly, at $U_{sk} = 0.53$ m/s and $U_{sw} = 0.07$ m/s, the percentage increase in pressure drop was 6.10 % at 0°, 12.58 % at 30° and 19.81 % at 45°.
- The experimental findings validate the numerical model. At $U_{sk} = 0.07$ m/s & $U_{sw} = 0.66$ m/s and $U_{sk} = 0.66$ m/s & $U_{sw} = 0.66$ m/s, the maximum deviation in pressure drop was 4.71 %, both of which are within the permissible range.

Funding

This study has been funded by Birla Institute of Technology, Mesra (grant no. GO/Estb/SMS/2020–21/2262).

Data availability statement

Data available on request from the authors.

CRediT authorship contribution statement

Mushtaque Momin: Writing – original draft, Visualization, Validation, Investigation, Formal analysis, Data curation, Conceptualization. **Faisal Rahmani:** Writing – review & editing, Supervision, Methodology, Conceptualization. **Emad Makki:** Software, Resources, Investigation, Formal analysis. **Mukesh Sharma:** Writing – review & editing, Supervision, Methodology, Formal analysis, Conceptualization. **Jayant Giri:** Visualization, Software, Resources, Data curation. **T. Sathish:** Visualization, Software, Resources, Data curation.

Declaration of competing interest

The authors declare the following financial interests/personal relationships which may be considered as potential competing interests:Mukesh Sharma reports financial support was provided by Birla Institute of Technology.

Nomenclature

U_{sk}	Superficial velocity of oils
U_{sw}	Superficial velocity of water
ρ	Density
V	Vector of velocity
t	Time
g	Acceleration due to Gravitational
μ	Dynamic Viscosity
F	Body Force
μ_t	Eddy Viscosity
n	Number Of Phases
α_q	Fraction Of qth Phase
I	Unit Tensor
$\otimes$	Symbol of tensor product of two vectors
ρ_{eq}	Mixture Density
U_{eq}	Mixture Velocity
μ_{eq}	Mixture Viscosity
∇P_{hydro}	Hydrodynamic Pressure Drop
A	Cross-sectional Area
A_i	Area covered by oil
U_r	Radial Velocity
U_x	Axial Velocity
D	Diameter of the U bend
p	Pressure

References

[1] M. Pietrzak, S. Witczak, Flow patterns and void fractions of phases during gas-liquid two-phase and gas-liquid-liquid three-phase flow in U-bends, Int. J. Heat Fluid Flow 44 (2013) 700–710, https://doi.org/10.1016/j.ijheatfluidflow.2013.09.007.

[2] Y. Amini, V. Ghazanfari, M. Heydari, M.M. Shadman, A.G. Khamseh, M.H. Khani, A. Hassanvand, Computational fluid dynamics simulation of two-phase flow patterns in a serpentine microfluidic device, Sci. Rep. 13 (2023), https://doi.org/10.1038/s41598-023-36672-6.

[3] W. Peng, X. Cao, L. Ma, P. Wang, J. Bian, C. Lin, Sand erosion prediction models for two-phase flow pipe bends and their application in gas-liquid-solid multiphase flow erosion, Powder Technol. 421 (2023), https://doi.org/10.1016/j.powtec.2023.118421.

[4] B. Hong, Y. Li, Y. Li, J. Gong, Y. Yu, A. Huang, X. Li, Numerical simulation of solid particle erosion in the gas-liquid flow of key pipe fittings in shale gas fields, Case Stud. Therm. Eng. 42 (2023), https://doi.org/10.1016/j.csite.2023.102742.

[5] S. Arirachakaran, O. Shoham, J.P. Brill, U. Of Tulsa, SPE SPE 18836 an Analysis of Oil/Water Flow Phenomena in Horizontal Pipes, 1989.

[6] J.L. Trallero, C. Sarica, J.P. Brill, A Study of Oil/Water Flow Patterns in Horizontal Pipes, 1997.

[7] D. Zhang, H. Zhang, J. Rui, Y. Pan, X. Liu, Z. Shang, Prediction model for the transition between oil–water two-phase separation and dispersed flows in horizontal and inclined pipes, J. Pet. Sci. Eng. 192 (2020), https://doi.org/10.1016/j.petrol.2020.107161.

[8] T. Al-Wahaibi, N. Yusuf, Y. Al-Wahaibi, A. Al-Ajmi, Experimental study on the transition between stratified and non-stratified horizontal oil-water flow, Int. J. Multiphas. Flow 38 (2012) 126–135, https://doi.org/10.1016/j.ijmultiphaseflow.2011.08.007.

[9] P. Poesio, D. Strazza, G. Sotgia, Very-viscous-oil/water/air flow through horizontal pipes: pressure drop measurement and prediction, Chem. Eng. Sci. 64 (2009) 1136–1142, https://doi.org/10.1016/j.ces.2008.10.061.

[10] M. Andrianto Deendarlianto, A. Widyaparaga, O. Dinaryanto, Indarto Khasani, CFD Studies on the gas-liquid plug two-phase flow in a horizontal pipe, J. Pet. Sci. Eng. 147 (2016) 779–787, https://doi.org/10.1016/j.petrol.2016.09.019.

[11] T. Al-Wahaibi, Pressure gradient correlation for oil-water separated flow in horizontal pipes, Exp. Therm. Fluid Sci. 42 (2012) 196–203, https://doi.org/10.1016/j.expthermflusci.2012.04.021.

[12] A.R. Hasan, N. Dakota, C.S. Kabir, A Simplified Model for Oil/Water Flow in Vertical and Deviated Wellbores, 1999.

[13] A.K. Jana, G. Das, P.K. Das, Flow regime identification of two-phase liquid-liquid upflow through vertical pipe, Chem. Eng. Sci. 61 (2006) 1500–1515, https://doi.org/10.1016/j.ces.2005.09.001.

[14] M. Du, N. De Jin, Z.K. Gao, Z.Y. Wang, L.S. Zhai, Flow pattern and water holdup measurements of vertical upward oil-water two-phase flow in small diameter pipes, Int. J. Multiphas. Flow 41 (2012) 91–105, https://doi.org/10.1016/j.ijmultiphaseflow.2012.01.007.

[15] J. yu Xu, D. hui Li, J. Guo, Y. xiang Wu, Investigations of phase inversion and frictional pressure gradients in upward and downward oil-water flow in vertical pipes, Int. J. Multiphas. Flow 36 (2010) 930–939, https://doi.org/10.1016/j.ijmultiphaseflow.2010.08.007.

[16] E. Adaze, H.M. Badr, A. Al-Sarkhi, CFD modeling of two-phase annular flow toward the onset of liquid film reversal in a vertical pipe, J. Pet. Sci. Eng. 175 (2019) 755–774, https://doi.org/10.1016/j.petrol.2019.01.026.

[17] X. Ma, M. Tian, J. Zhang, L. Tang, F. Liu, Flow pattern identification for two-phase flow in a U-bend and its contiguous straight tubes, Exp. Therm. Fluid Sci. 93 (2018) 218–234, https://doi.org/10.1016/j.expthermflusci.2017.12.024.

[18] J. López, N. Ratkovich, E. Pereyra, Analysis of two-phase air-water annular flow in U-bends, Heliyon 6 (2020), https://doi.org/10.1016/j.heliyon.2020.e05818.

[19] C.C. Wang, I.Y. Chen, Y.W. Yang, Y.J. Chang, Two-phase flow pattern in small diameter tubes with the presence of horizontal return bend, Int. J. Heat Mass Tran. 46 (2003) 2975–2981, https://doi.org/10.1016/S0017-9310(03)00071-1.

[20] S. Yadav, H.B. Mehta, Experimental investigations on air–water two-phase flow through a minichannel U-bend, Exp. Therm. Fluid Sci. 78 (2016) 182–198, https://doi.org/10.1016/j.expthermflusci.2016.05.019.

[21] A.M. Aliyu, A.A. Almabrok, Y.D. Baba, L. Lao, H. Yeung, K.C. Kim, Upward gas–liquid two-phase flow after a U-bend in a large-diameter serpentine pipe, Int. J. Heat Mass Tran. 108 (2017) 784–800, https://doi.org/10.1016/j.ijheatmasstransfer.2016.12.069.

[22] K. De Kerpel, S. De Schampheleire, T. De Keulenaer, M. De Paepe, Two-phase frictional pressure drop and flow behaviour up- and downstream of a sharp return bend, Appl. Therm. Eng. 93 (2016) 824–838, https://doi.org/10.1016/j.applthermaleng.2015.10.064.

[23] M. Sharma, P. Ravi, S. Ghosh, G. Das, P.K. Das, Studies on low viscous oil-water flow through return bends, Exp. Therm. Fluid Sci. 35 (2011) 455–469, https://doi.org/10.1016/j.expthermflusci.2010.11.007.

[24] M. Sharma, P. Ravi, S. Ghosh, G. Das, P.K. Das, Hydrodynamics of lube oil-water flow through 180° return bends, Chem. Eng. Sci. 66 (2011) 4468–4476, https://doi.org/10.1016/j.ces.2011.04.031.

[25] S. Ghosh, G. Das, P.K. Das, Simulation of core annular in return bends-A comprehensive CFD study, Chem. Eng. Res. Des. 89 (2011) 2244–2253, https://doi.org/10.1016/j.cherd.2011.03.015.

[26] N. Nandi, P. Dutta, Numerical analysis on the development of vortex structure in 90° pipe bend, Progress in Computational Fluid Dynamics, Int. J. 21 (2021) 261, https://doi.org/10.1504/PCFD.2021.10039615.

[27] P. Dutta, N. Nandi, Numerical study on turbulent separation reattachment flow in pipe bends with different small curvature ratio, J. Inst. Eng.: Series C. 100 (2019) 995–1004, https://doi.org/10.1007/s40032-018-0488-9.

[28] P. Dutta, H. Chattopadhyay, N. Nandi, Numerical studies on turbulent flow field in a 90 deg pipe bend, Journal of Fluids Engineering, Transactions of the ASME 144 (2022), https://doi.org/10.1115/1.4053547.

[29] Y. Kumar, D.R. Kaushal, Pipe bend erosion CFD modeling for two-phase liquid-solid slurry, in: Mater Today Proc, Elsevier Ltd, 2023, pp. 53–60, https://doi.org/10.1016/j.matpr.2022.11.340.

[30] S. Passoni, I.M. Carraretto, R. Mereu, L.P.M. Colombo, Two-phase stratified flow in horizontal pipes: a CFD study to improve prediction of pressure gradient and void fraction, Chem. Eng. Res. Des. 191 (2023) 38–49, https://doi.org/10.1016/j.cherd.2023.01.016.

[31] Lafaurie Bruno, Modelling merging and fragmentation in multiphase flow with SURFER, JOURNAL OF COMUPUTATIONAL PHYSICS 113 (1994) 134–147.

[32] S.V. Patankar, Numerical Heat Transfer and Fluid Flow, Hemisphere Pub. Corp., 1980.

[33] H. Montazeri, M. Bussmann, J. Mostaghimi, Accurate implementation of forcing terms for two-phase flows into SIMPLE algorithm, Int. J. Multiphas. Flow 45 (2012) 40–52, https://doi.org/10.1016/j.ijmultiphaseflow.2012.05.003.

[34] R.K. Verma, S. Ghosh, Effect of phase properties on liquid-liquid two-phase flow patterns and pressure drop in serpentine mini geometry, Chem. Eng. J. 397 (2020), https://doi.org/10.1016/j.cej.2020.125443.

[35] M. Pietrzak, Flow patterns and volume fractions of phases during liquid-liquid two-phase flow in pipe bends, Exp. Therm. Fluid Sci. 54 (2014) 247–258, https://doi.org/10.1016/j.expthermflusci.2013.12.024.